Final Draft

of the original manuscript

Shi, Q.-X.; Wang, C.-J.; Deng, K.-K.; Nie, K.-B.; Cao, M.; Gan, W.-M.; Liang, W.:

Work hardening and softening behavior of pure Mg influenced by Zn addition investigated via in-situ neutron diffraction.

In: Materials Science and Engineering: A. Vol. 772 (2020) 138827.

First published online by Elsevier: 14.12.2019

https://dx.doi.org/10.1016/j.msea.2019.138827

Work hardening and softening behavior of Pure Mg influenced by Zn addition investigated via in-situ neutron diffraction

Quan-xin Shi[a], Cui-ju Wang[a], Kun-kun Deng[a]*, Kai-bo Nie[a], Miao-Cao[a], Wei-min Gan[b]**

Wei-Liang[a]

[a]Shanxi Key laboratory of advanced magnesium-based materials, College of Materials Science and Engineering,Taiyuan University of Technology, Taiyuan 030024, PR China

[b]GMS at MLZ, Helmholtz-Zentrum Geesthacht, Garching Germany

Corresponding author. *E-mail: dengkunkun@tyut.edu.cn. (Kun-kun Deng)

**E-mail: weimin.gan@hzg.de (Wei-min Gan)

Abstract:

The work hardening and softening behavior of pure Mg influenced by Zn addition were studied through the neutron diffraction at STRESS-SPEC under *in-situ* tensile deformation. The measurement of line broadening evolution during *in-situ* tension was used to study the variation of dislocation density in pure Mg and Mg-5Zn alloy, which revealed the effect of dislocation on work hardening behavior. Meanwhile, the tensile stress reduction ($\Delta P_{i(i=1,2,3)}$) due to softening effect at different *in-situ* tensile deformation stages were calculated to analyze the effect of Zn addition on softening behavior. The results show that the work hardening rate of pure Mg is larger than that of Mg-5Zn alloy in the early stage of deformation because of the stronger effect of grain size on the work hardening behavior. But the work hardening rate of Mg-5Zn alloy is higher than that of pure Mg in the later stage of deformaiton, which is attributed to the stronger effect of precipitates on work hardening behavior. Moreover, ΔP_1 of pure Mg is larger than that of Mg-5Zn alloy, which was explained by the large grain size of pure Mg results in higher stored energy during the early deformation stage, and providing a

greater driving force for softening behavior. However, with the increase of tensile strain, the increase significantly of stored energy in Mg-5Zn alloy due to the dislocations migration hindered by precipitates during the tensile deformation, leading to a higher driving force for softening behavior in the later deformation stage. Thus, □P_3 of Mg-5Zn alloy is larger than that of pure Mg.

***Keywords*:** Microstructure; Work hardening rate; Softening; *In-situ* tensile; Neutrons diffracitons

1.Introduction

In view of the extremely low density, excellent specific strength and stiffness of Mg, it has aroused widely attentions in automobile and electronics fields [1,2]. However, the development of Mg and Mg alloys are limited enormously due to their poor ductility and low strength at room temperature.

The alloying treatment is one of feasible methods to improve the mechanical properties of Mg [3,4]. Once the stress overpass the yield strength (YS), the work hardening behavior happens during the subsequent deformation process, which is also called the “work hardening strengthening” [5]. Considering the lower stacking fault energy, the work hardening strengthening is thought to play an important role in Mg alloys [6]. However, the work hardening behavior is very complex owing to the limited available activated slipping systems [7,8]. The reasons are mainly related to the grain size [6,9,10], texture [9-11], strain rate [12] and precipitation [6,13].

Nevertheless, many works had been done on the work hardening behavior of Mg

alloys [6-14]. Liu et al. [6] studied the effect of Sc addition on the work hardening behavior of as-extruded ZK60 alloy, and the results showed that the work hardening rate of ZK60 alloy decreased due to grain refinement of Sc. The effects of grain size, texture and twins on mechanical properties and work-hardening behavior of AZ31 alloy were studied by Guo et al. [10], the results showed that the work hardening rate decreased with the decrease of grain size, while the texture strength of the basal plane has little effect on the work hardening rate. In addition, it has been reported that the addition of nano-Al_2O_3 particles into AZ31 alloy would not only helpful to the grain refinement, but also hinder the dislocation movement, which resulted in the higher work hardening rate and lower dynamic recovery [14]. Meanwhile, the work hardening rates of pure Mg and AZ31 alloy were compared in Ref. [14], it can be found that AZ31 alloy possesses higher work hardening rate than pure Mg, which is attributed to the solution strengthening resulting in the delay of dynamic recovery.

It is noted that the researches on the work hardening behavior of Mg alloys are mainly based on the tensile curve at room temperature. However, it is generally accepted that the work hardening and dynamic softening occur simultaneously during deformation. Then, in order to obtain the improved mechanical properties of industrial productions, the softening behavior should be also considered and studied. Li et al. [15] investigated the static softening characteristics and static recrystallization kinetics of A6082 Al alloy, and interpreted that the softening mechanisms were static recovery and static recrystallization. Jiang et al. [16,17] found that static recovery was the principal static softening contribution in 7150 Al alloy by combining experimental and modeling

works. Chen et al. [18] also studied the static softening behavior of Al-Zn-Mg-Cu alloy during interval holding of double-stage hot deformation by calculating the softening fraction. However, little studies concentrated on the work hardening and softening behavior of Mg alloys simultaneously at different deformation stages.

To clarify the effect of alloying elements on the work hardening and softening behavior of Mg matrix simultaneously, the pure Mg and Mg-5Zn alloy are selected and subjected to the *in-situ* tensile tested by neutron diffraction. Through investigating the evolution of line broadening (defect evolution) as well as the changing of stress during softening process of pure Mg and Mg-5Zn alloy, the work hardening and softening behavior of Mg matrix influenced by Zn elements during tensile process will be understood and discussed in detail in this work.

2. Experience procedures

The pure Mg and pure Zn were chosen by melting at 750^{o}C to product the Mg-5 wt.%Zn alloy, and the whole melting process was conducted in the protection of a mixted atmosphere of CO_2 and SF_6. The as-casted Mg-5 wt.%Zn was homogenized at 320^{o}C for 8h firstly, and subsequently held at 430^{o}C for 16h. Then, Mg-5Zn alloy was water quenched as quickly as possible. The as-solutioned Mg-5Zn alloy was extruded at 200 ^{o}C with a speed of 0.1mm/s, and the extrusion ratio is 16:1. At last, the extruded bars with a diameter of 10mm were obtained. Pure Mg was also extruded at the same condition as a comparison.

The optical microscope (OM), scanning electron microscope (SEM), transission electron microscope (TEM) and electron backscattered diffraction (EBSD) were used

to anlyze the microstructure and microtexture of pure Mg and Mg-5Zn alloy. The samples of OM and EBSD were cut along the extrusion direction (ED). The OM samples were ground using the emery papers firstly, and then etched in a solution of an oxalic acid (2g oxalic acid + 50 mL distilled water) to reveal the grain boundaries. The EBSD samples were prepared by grinding on the different emery papers, then followed by electro-polished with the 5% perchloric acid solution at -30^{o}C for 1.5min. The dates from the EBSD were analyzed by using the channel 5 software. The SEM combined with EDS and XRD were used to identify the chemical compositions of the secondary phases in Mg-5Zn alloy. The ex-tensile samples, with the gauge length of 25mm, and the cross-section of 6mm × 2mm, were performed along the ED at room temperature on a MTS-E45.105 test machine with a tensile speed of 0.5mm/min.

The *in-situ* tensile experiment were performed under a loading rate of 10N/s using the unique tesile rig at STRESS-SPEC (MLZ, Garching), and the dimensions of the *in-situ* tensile test speciments are d_o=5mm, L_o=25mm, d_1=M8, L_c=30mm and L_t=50mm. The experimental setup is shown in Fig. 1. The loading direction of the *in-situ* tensile test was parallel to the extrusion direciton of the samples. The line broadening (defect evolution) of the different crystal planes for pure Mg and Mg-5Zn alloy were measured during the *in-situ* tensile test when the tension displacement remains unchanged (a called position control mode). Meanwhile, the bulk texture of the as-extruded pure Mg and Mg-5Zn alloy were also measured ex-situ by neutron diffraction. In addition, the effect of Zn addition to pure Mg on work hardening and softening behavior were studied by calculating the stress reduction ($\triangle P_{i(i=1,2,3)}$) at different deformation stages of *in-situ*

tensile process.

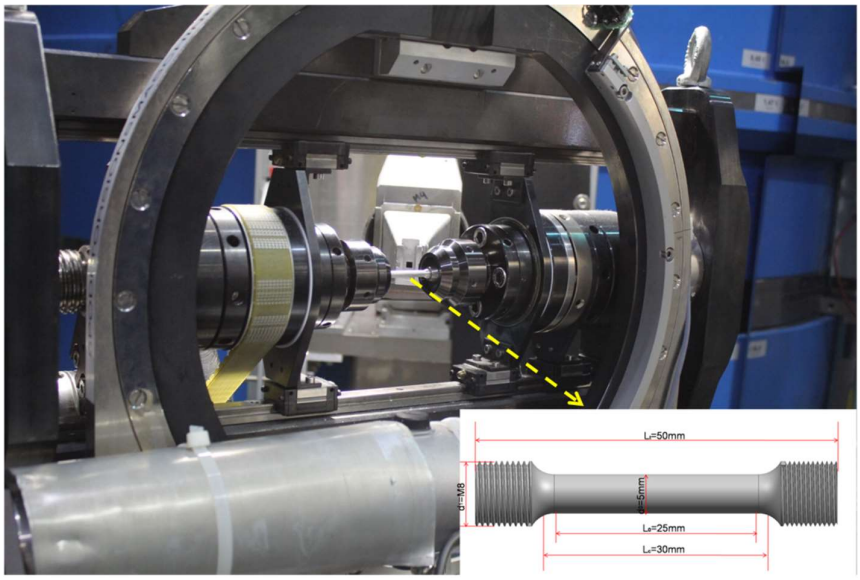

Fig. 1. In-situ stretching equipment and sample diagram

3. Results

3.1 Microstructure of the as-casted Mg-5Zn alloy

Fig. 2 shows the OM, SEM and EDS of the as-cast and as-homogenized Mg-5Zn alloy. It can be seen from Fig. 2(a) and Fig. 2(b) that the average grains size of the as-cast Mg-5Zn alloy is ~96.54μm and the secondary phases in which are distributed in the grains and along the grain boundaries. The results of EDS analysis of the secondary phase in as-cast Mg-5Zn alloy show that the atomic ratio of Mg/Zn is about 7:3, indicating the second phase may be Mg_7Zn_3 [19].

After the homogenization treatment, the average grains size of Mg-5Zn alloy increased to ~171.6μm, as shown in Fig. 2(d)(e)(f). Meanwhile, the results of SEM and EDS analysis show that the secondary phases in as-cast Mg-5Zn alloy are almost completely dissolved into the matrix alloy.

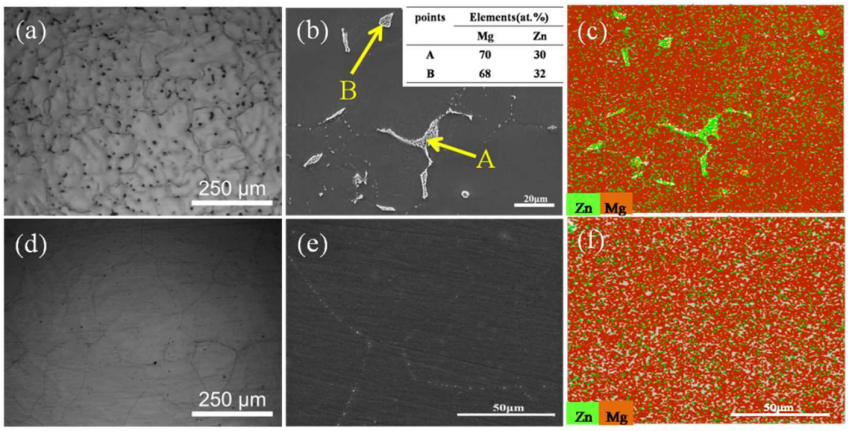

Fig. 2. OM (a), SEM (b) and EDS (c) of as-casted Mg-5Zn alloy and OM (d), SEM (e) and EDS (f) of as-homogenized Mg-5Zn alloy

3.2 Microstructures of the as-extruded pure Mg and Mg-5Zn alloy

The OM microstructure of the as-extruded pure Mg and Mg-5Zn alloy were shown in Fig. 3. Compared with Fig. 2(d), it can be found that a high fraction of fine DRXed grains were formed in Mg-5Zn alloy after extrusion deformation in addition to the deformed grains elongated along the extrusion direction, and the twins can also be recognized in Fig. 3(c). The average DRXed grains size and DRXed ratio of the as-extruded Mg-5Zn alloy are about 4.11μm and 85.31%, respectively. However, the DRXed ratio is close to 100% and the average DRXed grains reaches to ~11.89μm for the as-extruded pure Mg, as shown in Fig. 3(a) and Fig. 3(b). Thus, compared with extruded pure Mg and Mg-5Zn alloy, the Zn element seems to inhibit the DRX of Mg matrix.

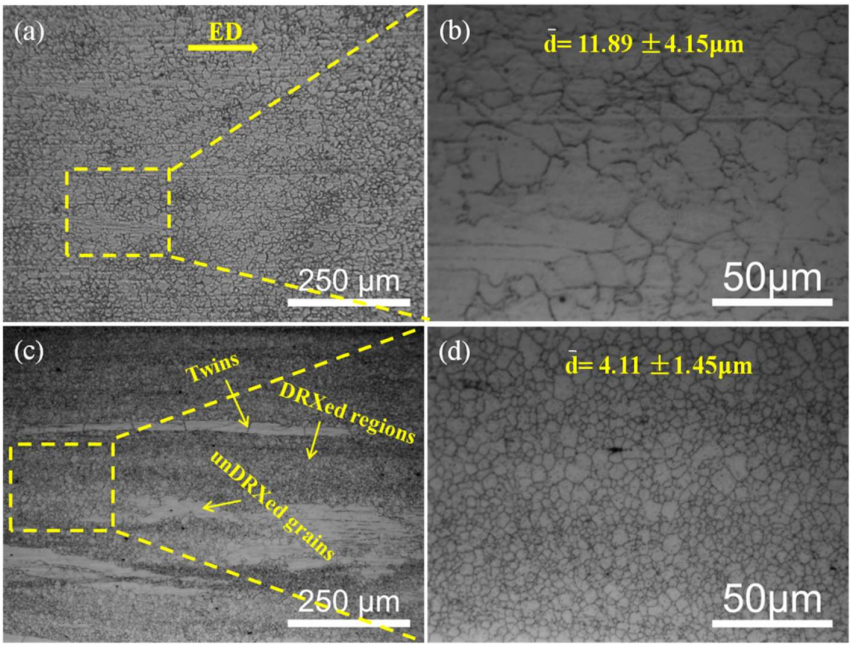

Fig. 3. OM microstructure of as-extruded pure Mg (a)(b) and Mg-5Zn alloy (c)(d)

The SEM, XRD and EDS results of the as-extruded Mg-5Zn alloy are given in Fig. 4. As compared with Fig. 2(e), a lot of white fine and dense precipiates are found in the as-extruded Mg-5Zn alloy, which indicates that precipitates were dynamically formed from the as-homogenized Mg-5Zn alloy during extrusion, as shown in Fig. 4(a). The composition of precipitates at grain boundaries (points A and B) and in grains (point C) were measured by EDS (Fig. 4(b)). The results show that there are two elements of Mg and Zn in the precipitates (Fig. 4(d)). Further component analysis by XRD in Fig. 4(c) shows that the as-extruded Mg-5Zn alloy contains $MgZn_2$ phase besides α-Mg phase, thus it is determined that the dynamic precipitates in Mg-5Zn alloy during extrusion is $MgZn_2$ phase. Meanwhile, the measured average size and volume fraction of $MgZn_2$ are 125nm and 1.04%, respectively, in the as-extruded Mg-5Zn alloy.

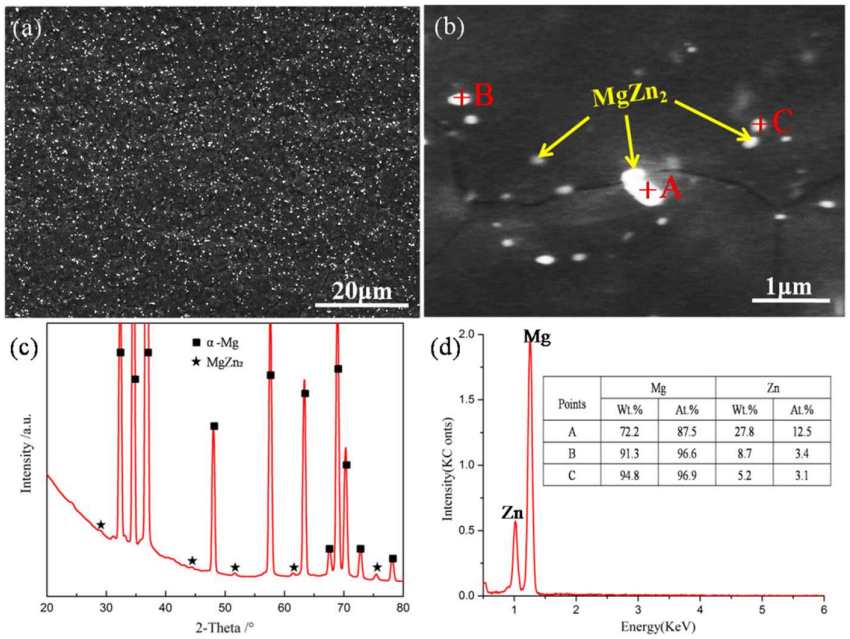

Fig. 4. SEM (a)(b), XRD (c) and EDS of precipitates (d) of as-extruded Mg-5Zn alloy

TEM microstructure of the as-extruded Mg-5Zn alloy are given in Fig. 5. High density dislocations can be found in Fig. 5(a). Besides, there are also many spherical precipitates embedded among these dislocations. Based on the selective diffraction patterns in Fig. 5(b), these precipitates should be $MgZn_2$ phase, which is consist with the analysis in Fig. 4. The DRX process relate to the movement of dislocations, which usually evolve into dislocation cells and sub-grain boundaries, and finally develop to the DRXed grains. However, the precipitated $MgZn_2$ phase will hinder the movement of both dislocations and grain boundaries, which inevitable delay the occurrence of DRX process and the growth of DRXed grains [20]. Therefore, both the average DRXed grains size and DRXed ratio of Mg-5Zn alloy are less than that of pure Mg.

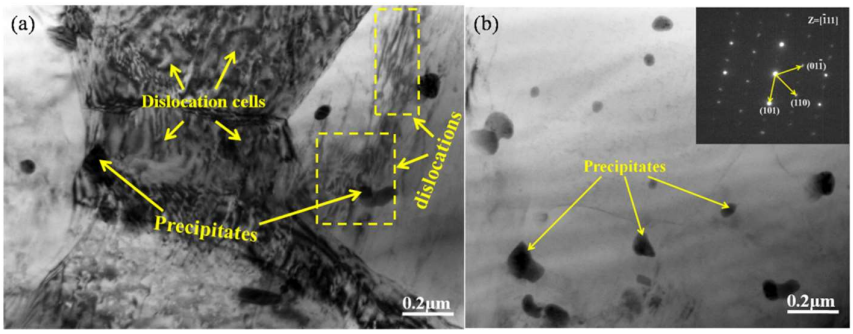

Fig. 5. TEM microstructure of as-extruded Mg-5Zn alloy (a) and diffraction pattern of the precipitates in Mg-5Zn alloy (b)

3.3 Texture

Fig. 6 depicts the EBSD results of the as-extruded pure Mg and Mg-5Zn alloy. It can be seen from IPF maps that the colors of the grains in the as-extruded pure Mg are mainly blue and green, which indicate $\{10\bar{1}0\}$ oriented grains and $\{11\bar{2}0\}$ oriented grains, respectively. However, the colors of the grains in Mg-5Zn alloy are not only bule and green, but also a small amount of red, which means {0002} oriented grains. Then, it can be concluded that the orientation of some grains was changed due to the addition of Zn into pure Mg. Moreover, more twins can be seen in the as-extruded Mg-5Zn alloy, as shown in Fig. (3) and Fig. (6). It can be observed from the misorientation distribution maps of as-extruded pure Mg and Mg-5Zn alloy, besides the peak at 30° caused by the typical fiber texture formed by the extrusion deformation, the peak also appears at about 86° (Fig. 6(b) and Fig. 6(e)). It can be concluded that the twins formed in the as-extruded Mg-5Zn alloy may be the 86°$\{11\bar{2}0\}$ tensile twins.

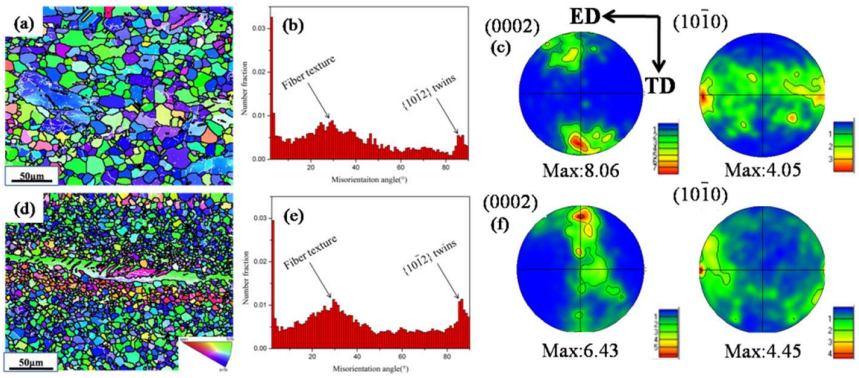

Fig. 6. IPF, misorientation angle distribution and texture for as-extruded pure Mg (a)(b)(c) and Mg-5Zn alloy (d)(e)(f)

According to Kim et al's investigation [21], a large amount of strain energy accumulates in the twin bands during the deformation process, which will provide the favorable sites for the nucleation of DRXed grains. Therefore, the formation of the red-orientation DRXed grains in Mg-5Zn alloy may be explained by the fact that the twins induce the occurrence of DRX during extrusion, and resulting in the rotation of the DRXed grains orientation.

The textures distribution of pure Mg and Mg-5Zn alloy measured by EBSD are shown in Fig. 6(c) and Fig. 6(f). The sharp <10$\bar{1}$0> fiber texture (TD texture) can be observed in pure Mg and Mg-5Zn alloy, and the intensity of basal plane texture are 8.06 mrd and 6.43 mrd, respectively. It should be note that the texture measured by EBSD is relatively microscopic because of its limit area. In this work, the bulk texture of the as-extruded pure Mg and Mg-5Zn alloy were measured by neutron diffraction, which are shown in Fig. 7. As the same as Fig. 6, the strong <10$\bar{1}$0> fibre texture can also be found in the pole figures of pure Mg and Mg-5Zn alloy. Moreover, the intensity of basal plane texture for pure Mg and Mg-5Zn alloy are are 4.27 mrd and 3.30 mrd, respectively. That means the addition of Zn element can weaken the texture of Mg matrix.

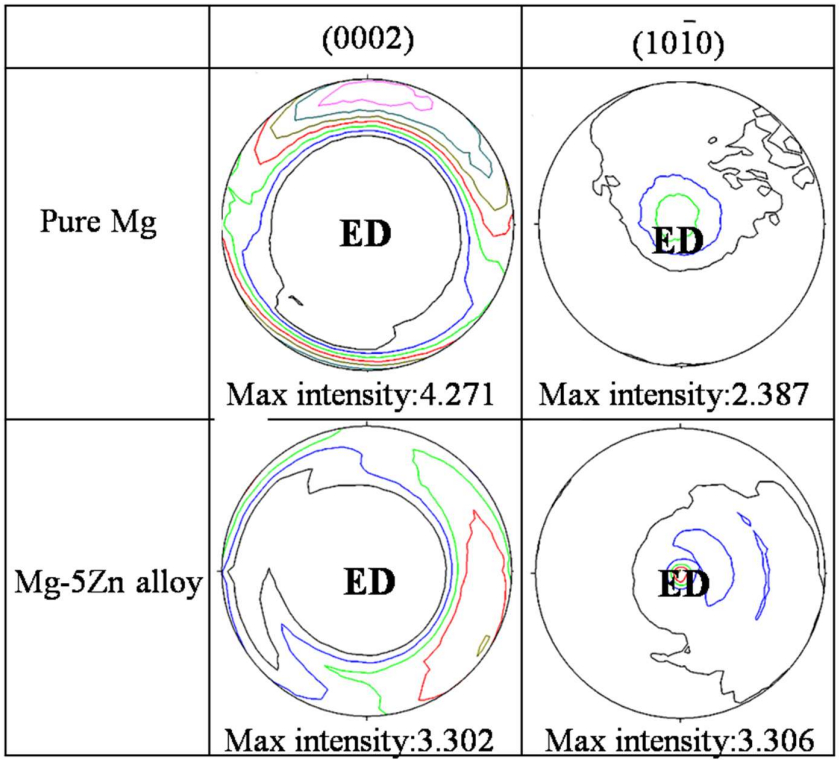

Fig. 7. Macro-texture of as-extruded pure Mg and Mg-5Zn alloy

It is generally accepted that the intensity of texture can be influenced by DRXed ratio, grains size and the second phases of Mg alloy. As seen from Fig. 3, DRXed ratio of the as-extruded Mg-5Zn alloy is lower than that of pure Mg, and the average DRXed grains size of Mg-5Zn alloy is also smaller than that of pure Mg. The smaller of the grain is, the more random of the grain orientations are [22]. The IPF map and distribution of basal texture of as-extruded Mg-5Zn alloy with the grain size smaller than the average DRXed grains are shown in Fig. 8. It can be found that the maximum intensity of the basal texture is 4.64 mrd, which is lower than that of as-extruded Mg-5Zn alloy with fulled grains (6.43 mrd). Thus, the weaken basal texture for Mg-5Zn alloy can be explained by its large proportion of fine DRXed grains.

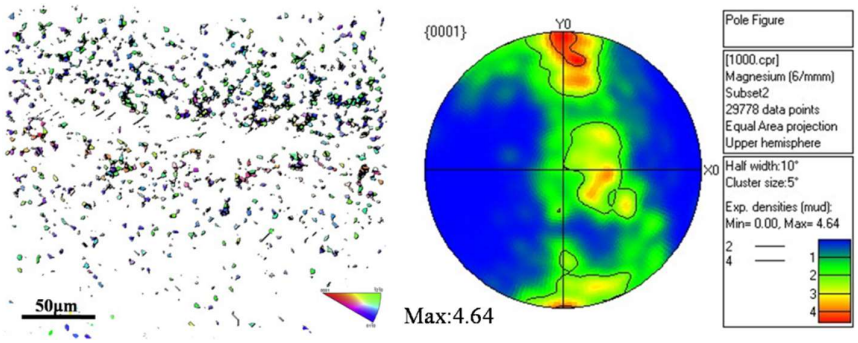

Fig. 8. IPF (a) and basal plane texture (b) of as-extruded Mg-5Zn alloy with the grains size smaller than the average grains size

Meanwhile, a large number of fine dynamic precipitated $MgZn_2$ phase can also be observed in as-extruded Mg-5Zn alloy, as shown in Fig. 5. According to Ref. [19], the secondary phase precipitate during extrusion process will pin grain boundaries and hinder the rotation of grain toward basal orientaion, which resluts in a weak basal plane texture. Furthermore, the non-basal plane texture (ND textrure) can be formed by the twins in the Mg-5Zn alloy (Fig. 6(f)), which further weaken the basal plane texture [23,24].

3.4 Mechanical properties

Fig. 9(a) shows the stress-strain curve of the as–extruded pure Mg and Mg-5Zn alloy at room temperature. It is intersting to note that the addition of Zn element plays a great role in the mechanical properties of pure Mg. The YTS, UTS and elongation of pure Mg are 107.71MPa, 158.4MPa and 8%, respectively. However, the YTS, UTS and elongation of Mg-5Zn alloy increased to 146.13MPa, 263.26MPa and 17.27%, respectively. Therefore, the YTS, UTS and elongation of pure Mg can be improved obviously by adding Zn. The reasons may attribute to the fine DRXed grains as well as a large amount of precipitated $MgZn_2$ phase in the as-extruded Mg-5Zn alloy.

Besides, the tensile fracture morphologies of Mg-5Zn alloy and pure Mg are given in Fig. 9(b) and Fig. 9(c). It can be found that more fine circular dimples can be seen on the surface of Mg-5Zn fracture, which indicates the better ducility of Mg-5Zn alloy.

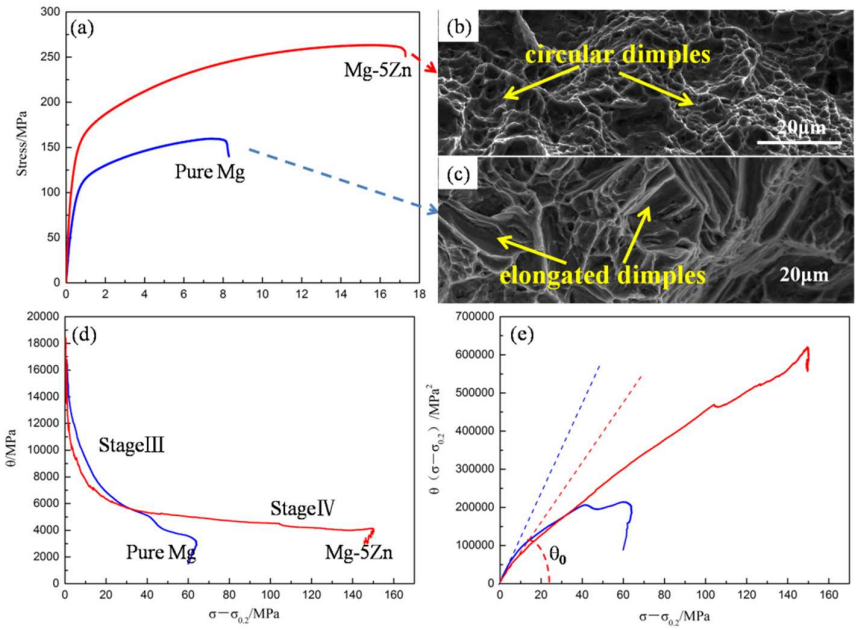

Fig. 9. Tensile stress-strain curves (a), fracture morphology (b)(c), work hardening rate (θ) (d) and the plot of $(\sigma-\sigma_{0.2})\theta$ vs. $(\sigma-\sigma_{0.2})$ (e) for as-extruded pure Mg and Mg-5Zn alloy

Fig. 10 shows the (0001)/<11$\bar{2}$0> basal slip Schmid factors maps of the as-extruded pure Mg and Mg-5Zn alloy through the EBSD analysis. It can be seen from Fig. 10(a) that the grains of pure Mg after the extrusion are mainly blue and green with low Schmid factor. As seen from the distribution of (0001)/<11$\bar{2}$0> basal slip Schmid factors of pure Mg (Fig. 10(b)), the average value of the Schmid factors is ~0.2. However, a large number of red grains with large Schmid factor are observed in Mg-5Zn alloy (Fig. 10(c)). The distribution and the average value of Schmid factors of Mg-5Zn alloy is shown in Fig. 10(d), the the average value of Schmid factors is ~0.37, which is significantly higher than that of pure Mg (0.2). It is widely acknowledged that the basal slip is the main deformation mechanism for Mg alloys, so the Schmid factor

value of (0001)/<11$\bar{2}$0> slip can be used to assess the difficult degree of basal slip activation [25]. The high average schmid factors means that the basal slip is easier to start under applied stress, leading to high ductility for Mg alloys [25]. Obviously, the higher average Schmid factors value of Mg-5Zn alloy gives it better ductility.

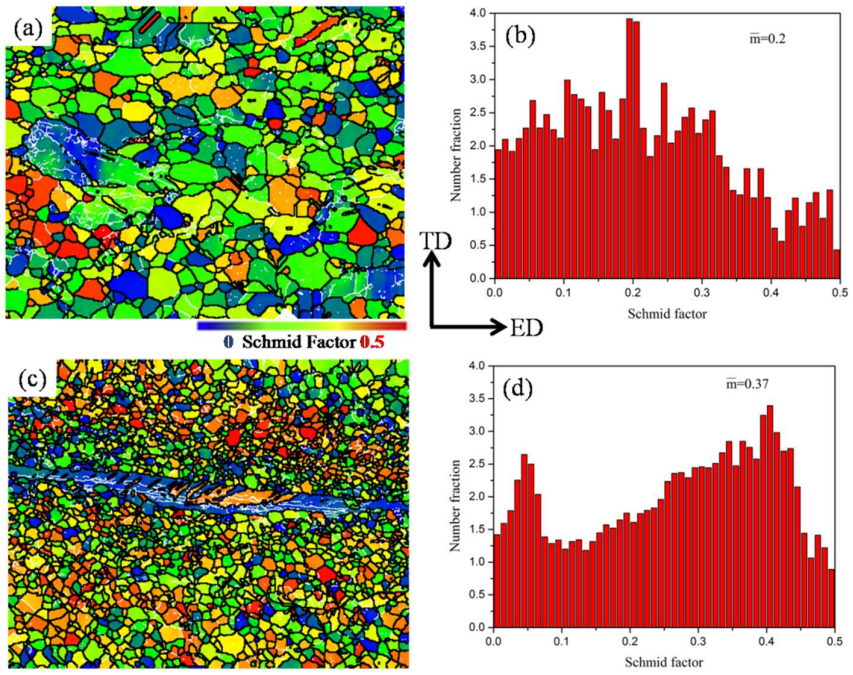

Fig. 10. (0001)/<11$\bar{2}$0> basal slip Schmid factors maps of as-extruded pure Mg (a)(b) and Mg-5Zn alloy (c)(d)

The work hardenging behavior of materials can be expressed by the Eq. (1) [6]:

$$\theta = \partial\sigma / \partial\varepsilon \qquad (1)$$

where σ and ε are true stress and strain, respectively. Fig. 9(d) shows the work-hardening curves θ vs. (σ-$\sigma_{0.2}$) for as-extruded pure Mg and Mg-5Zn alloy. As observed from Fig. 9 (d), there is no stageIIcan be seen, but the dynamic recoverty stage (stage Ⅲ) and large-strain work hardening stage (stage IV) appear in the θ vs. (σ-$\sigma_{0.2}$) curves of present work.

The value of θ decreases sharply with the increase of flow stress at stage Ⅲ for

pure Mg and Mg-5Zn alloy, which is relate to the dynamic recovery. The work hardening rate θ of pure Mg is higher than that of Mg-5Zn alloy at stage Ⅲ. Meanwhile, the curve $(\sigma-\sigma_{0.2})\theta$ vs. $(\sigma-\sigma_{0.2})$ of pure Mg and Mg-5Zn alloy are given in Fig. 9(e). The slope θ_0 demonstrates the dynamic recovery rate of pure Mg and Mg-5Zn alloy at stage Ⅲ. It can be found from Fig. 9(e) that the θ_0 of pure Mg is higher than that of Mg-5Zn alloy, which means the high dynamic recovery rate of pure Mg.

Stage Ⅳ is the large-strain work hardening stage, which indicates the formation of dislocation cell structure [26,27]. It had been reported that the larger the grain size, the weaker the interaction between dislocation and grain boundary, resulting in the hardly formation of dislocation cells structure. Therefore, the starting point of the stage Ⅳ of pure Mg is not obvious relative to Mg-5Zn alloy. Moreover, it can be seen from Fig. 9(d), the work hardening rate at stage Ⅳ of Mg-5Zn alloy is significantly higher than that of pure Mg.

4. Discussions about the work hardening behavior and softening mechanism of pure Mg influenced by Zn addition

It is generally accepted that the work hardening behavior and dynamic softening mechanism are accompanied with each other during the deformation of the metal materials [18]. Macroscopicly, work hardening can make the flow stress of material increase with the increase of strain, while dynamic softening can counteract the increase of partical flow stress during plastic deformation. Microscopically, work hardening and dynamic softening relate to the storage and annihilation of dislocation, respectively. Therefore, the work hardening is mainly influenced by grain size and dislocation

density of the material, and the softening mechanism mainly includes recovery and recrystallization at the same deformation conditions. Considering the tensile test of the as-extruded pure Mg and Mg-5Zn alloy were performed at room temperature. Thus, the recrystallization is negligible in present work.

4.1 Work-hardening behavior

Once the stress overpass the YS, the work hardening occurs in Mg alloy, which results in the improvement of strength. Usually, the degree of work hardening can be described by work hardening capacity (*Hc*), which can be expressed by Eq. (2) [28,29]:

$$\mathrm{Hc} = \frac{\sigma_b^{\mathrm{true}} - \sigma_{0.2}^{\mathrm{true}}}{\sigma_{0.2}^{\mathrm{true}}} \quad (2)$$

where $\sigma_{0.2}^{true}$ and σ_b^{true} are the true yield strength and the true ultimate tensile strength, respectively. The $\sigma_{0.2}^{true}$ and σ_b^{true} of the as-extruded pure Mg are 108.53MPa and 169.14MPa, respectively; while the $\sigma_{0.2}^{true}$ and σ_b^{true} of the as-extruded Mg-5Zn are 146.99MPa and 303.34MPa, respectively. Then, the Hc values of pure Mg and Mg-5Zn alloy can be obtained by Eq. (2), which are 0.56 and 1.06, respectively. Therefore, the exsitence of Zn element is beneficial to improvement of the work hardening capacity for Mg matrix. The reasons may relate to dislocation interaction and strain hardening behavior after yielding [28,30]. To understand the strain-hardening behavior of pure Mg and Mg-5Zn alloy clearly, it is necessary to calculate their work hardening exponent [31].

The work hardening exponent *n* is a performance index to characterize the work hardening behavior of materials during the homogeneous plastic deformation, which can be calculated by the following Eq. (3), Eq. (4) and Eq. (5) [32]:

$$n = 0.035 + a + \sqrt{a^2 - 0.5\ln(\sigma_{0.2}/\sigma_b)} \quad (3)$$

$$a = 5 + 2\ln\varepsilon_s/8 \quad (4)$$

$$\varepsilon_s = \frac{\sigma_{0.2}}{E} + 0.002 \quad (5)$$

in which σ_b and $\sigma_{0.2}$ are UTS and YTS of materials, E is the elastic modulus and it is ~45GPa in present work. According to Eq. (3), the calculated work hardening exponents of pure Mg and Mg-5Zn alloy are 0.035 and 0.045, respectively. Usually, high n value indicates stronger work hardening effect [33]. The as-extruded Mg-5Zn alloy has higher work hardening effect than pure Mg, which is consistent with the work hardening curve. As compared with the pure Mg, the high Hc and n of Mg-5Zn alloy demonstrate its better work hardening strengthening effect. The reasons may associate with the texture, grain size and precipitates in the experimental samples.

The effect of texture on mechanical properties and work hardening behavior of AZ31 Mg alloys was studied by Guo et al. [10], it is found that the intensity of basal texture has little effect on work-hardening rate. Moreover, there is little difference in the basal texture intensity between pure Mg and Mg-5Zn alloy in present study, so the effect of texture on the work-hardeing behavior can be neglected.

Besides, Liu et al. [6] added Sc into ZK60 alloy and then the work hardening behavior of ZK60-SC alloy was invesitaged, the results show that the decreasing grains size would low down the work hardening rate of ZK60-Sc alloy even if the amount of Sc in which is increasing. In this work, the average grains size of the as-extruded Mg-5Zn alloy is finer than that of pure Mg (Fig. 3), which may account for the lower work

hardening rate of Mg-5Zn alloy as compared with pure Mg at stage Ⅲ (Fig. 9(d)).

On the contrary, the work hardening rate of Mg-5Zn alloy is higher than pure Mg once the tensile process proceed into stage IV, as shown in Fig. 9(d). Generally speaking, the plastic deformation of metal is realized by the dislocation slip, which relate to the movement of dislocation and the change of dislocation density [11]. Therefore, the dislocation stress field will affect the work hardening effect in the subsequent deformation process. The interaction among dislocations will lead to work hardening. The effect of work hardening caused by dislocation can be expressed by the Taylor equation as follow Eq. (6) [9,29]：

$$\sigma_d = M\alpha Gb\rho^{1/2} \quad (6)$$

where σ_d the contribution of dislocation density to flow stress; M the Taylor factor; α the constant; G the shear modulus; b the Burgers vector and ρ the dislocation density. Eq. (6) can be written as $\sigma_d \propto \rho^{1/2}$, which means that σ_d is proportional to $\rho^{1/2}$ [9]. Therefore, the increasing dislocation density will result in the improvement of the work hardening behavior of Mg alloys.

It is known that the precipitated phase can be regarded as the strong barries for dislocation slip, resulting in the improvement of the work hardening behavior [29]. Zhang et al. [13] have found that the strain hardening rate of SiC_p/Mg-*x*Al-2Ca composites increase with the increasing Al content due to the increased amount of precipitated phase. Meanwhile, abundant of researches have been studied about the evolution and hardening of precipitates in Mg alloys using computational model [34-37]. Fan et al. [35] studied and compared the hardening effect of plate-like, spherical

and rod-like precipitates on Mg alloys using molecular dynamics (MD) simulations and precipitation hardening model, the results show that the spherical precipitation phases have the strongest hardening effect. Besides, the interface strain has an important influence in the sequence of precipitates in Mg alloys according to the study of Wang et al. [37]. Solomon et al. [34] also analyzed the evolution of precipitates in Mg-Y alloys during aging treatment, the results indicate that the misfit strains promotes the evolution of the volume fraction of the precipitates, leading to the precipitate hardening for Mg-Y alloys.

In this work, a large number of fine $MgZn_2$ phases were produced in the as-extruded Mg-5Zn alloy based on the Section 3.2, which will hinder the movement of the dislocations during tensile deformation, then affecting work hardening behavior.

The evolution of the line broadening (defect evolution, FWHM, full width at half maximum) of the as-extruded pure Mg and Mg-5Zn alloy during tensile process are dispalyed in Fig. 11. It can be found that the FWHM values of (10.0), (10.1) and (11.0) planes in Mg-5Zn alloy are all higher than that of pure Mg when the tensile load is 0KN, which indicates that the density of defects in the as-extruded Mg-5Zn alloy is higher than that of pure Mg. Moreover, the FWHM values of (10.0), (10.1) and (11.0) planes of pure Mg and Mg-5Zn alloy are nearly no change during early stage of tensile. The main reason is that new defects cannot be formed during the elastic deformation stage, so the values of FWHM does not increase significantly. As the stress overpass the YTS, the dislocation density increases accompanied with the tensile process. Therefore, the value of FWHM increases significantly in both pure Mg and Mg-5Zn alloy. Even so,

the FWHM values of (10.0), (10.1) and (11.0) planes in Mg-5Zn alloy increase much more rapid than that of pure Mg during the plastic deformation process.

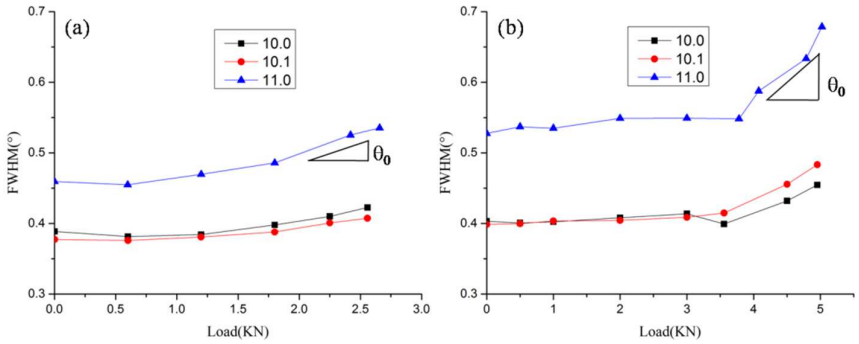

Fig. 11. The evolution of FWHM against tensile load for pure Mg (a) and Mg-5Zn alloy (b)

Above phenomenon indicate that the dislocation density in Mg-5Zn alloy before and after *in-situ* tensile deformation are significantly higher than that of pure Mg, so it can be proved that the work hardening caused by dislocation in Mg-5Zn alloy is larger than that of pure Mg. The reason mainly relates to the $MgZn_2$ phase precipitated in Mg-5Zn alloy, which hinders the migration of dislocations and enhances the work hardening effect. Even though the exsitence of $MgZn_2$ phase has the hinder effect on dislocation movement and results in the increasing work hardening rate, the work hardening rate of Mg-5Zn alloy is lower than that of pure Mg at the initial stage of plastic deformation (stage III). That should be relate to the softening behavior of Mg matrix influenced by Zn element during tensile process, which will be discussed in detail in the following part.

4.2 Softening behavior

The *in-situ* tensile stress-strain diagrams of the as-extruded pure Mg and Mg-5Zn alloy are shown in Fig. 12(a) and Fig. 12(d), respectively. It illustrates that the stress drops sharply when the tensile displacement is kept constant during *in-situ* tensile test.

Such phenomenon indicates the occurrence of softening. The magnified images of Fig. 12(a) and Fig. 12(d) are given in Fig. 12(b) and Fig. 12(e), respectively. However, the dropped stress is different for the pure Mg and Mg-5Zn alloy at different strains. That means the extent of softening is changing during the tensile process. To describe above phenomenon clearly, the dropped stress at different strains can be expressed by $\Delta P_{i(i=1,2,3)}$, which are exhibited in Fig. 12(c) and Fig. 12(f) for pure Mg and Mg-5Zn alloy, respectively. The abscissa positions of P_1, P_2 and P_3 in Fig. 12(c) and Fig. 12(f) are expressed by ε_{ri}, which can be described by Eq. (7):

$$\varepsilon_{ri} = \frac{\varepsilon_{i(i=1,2,3)} - \varepsilon_{0.2}}{\varepsilon_f - \varepsilon_{0.2}} \quad (7)$$

where $\varepsilon_{i(i=1,2,3)}$ are the strain values of P_1, P_2 and P_3 in pure Mg and Mg-5Zn alloy during in-situ tensile test, respectively. The $\varepsilon_{0.2}$ indicates the strain of YTS and the ε_f is the strain correspond to the fracture strength. The values of $\varepsilon_{i(i=1,2,3)}$, $\varepsilon_{0.2}$ and ε_f for pure Mg and Mg-5Zn alloy are shown in Table 1. Thus, the ε_{r1}, ε_{r2} and ε_{r3} of both pure Mg and Mg-5Zn alloy are calculated by Eq. (7) as ~0.25, ~0.50 and ~0.75, respectively. Meanwhile, the values of the $\Delta P_{i(i=1,2,3)}$ for pure Mg and Mg-5Zn alloy are also displayed in Table 1.

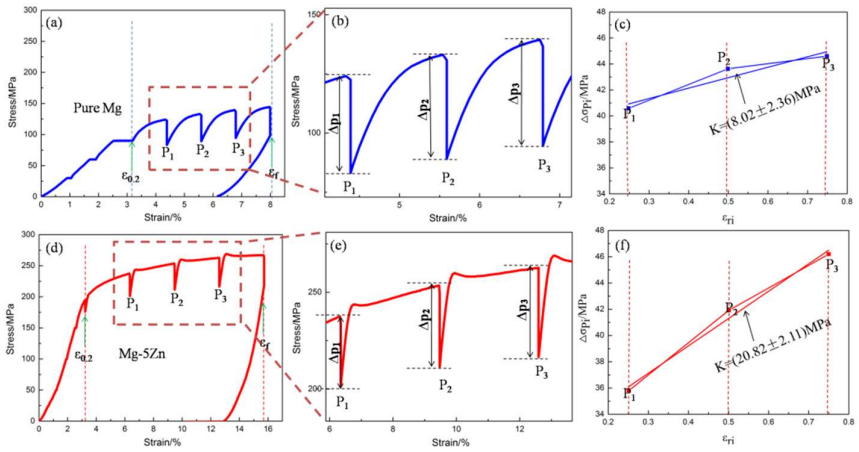

Fig. 12. In-situ tensile curves for as-extruded pure Mg and Mg-5Zn alloy: low magnification (a)(d), high magnification (b)(e) and variation of $\triangle P_i$ against ε_{ri}(c)(f)

Table 1. The values of $\varepsilon_{i(i=1,2,3)}$, $\varepsilon_{0.2}$, ε_f and $\Delta P_{i(i=1,2,3)}$ for pure Mg and Mg-5Zn alloy

Materials	ε_1	ε_2	ε_3	$\varepsilon_{0.2}$	ε_f	ΔP_1(MPa)	ΔP_2(MPa)	ΔP_3(MPa)
Pure Mg	4.3	5.6	6.8	3.2	8.1	40.58	43.62	44.6
Mg-5Zn	6.34	9.47	12.59	2.6	15.9	35.8	41.92	46.19

As seen from Table 1 and Fig. 12, the $\Delta P_{i(i=1,2,3)}$ of both pure Mg and Mg-5Zn alloy increase continuously during the whole in-situ tensile process. Despite that, it is interesting to note that the ΔP_1 and ΔP_2 of Mg-5Zn alloy are lower than that of pure Mg, however, the ΔP_3 of Mg-5Zn alloy are higher than that of pure Mg. The softening degree relates to ΔP_i and ε_{ri}, which can be expressed by Eq. (8):

$$K = \partial(\triangle P_i) / \partial(\varepsilon_{ri}) \quad (8)$$

Through Eq. (8), the values of K in pure Mg and Mg-5Zn alloy are 8.02MPa and 20.82MPa, respectively. The K value of Mg-5Zn alloy is about three times of pure Mg, it means the softening degree is increasing rapidly in Mg-5Zn alloy during the subsequent tensile process. The difference of softening process between pure Mg and Mg-5Zn alloy may also relate to the grain size and precipitated phases.

It should be noted from Section 3.1 that the Mg-5Zn alloy possesses the much finer DRXed grains than pure Mg. As compared with fine grains, the coarse grains will be propitious to the accumulation of dislocations [38]. The accumulated dislocations will generate large stress concentration at the grain boundaries of coarse grains, which makes it easy for the dislocation initiation at adjacent grains, it is in turn beneficial to

the transmission of slip and leading to the release of dislocations accumulation.

Considering the coarse grains in pure Mg, the $\triangle P_1$ value of which is larger than that of Mg-5Zn alloy in the initial stage of in-situ tensile deformation. However, the fine precipitates in Mg-5Zn alloy will inevitably hinder the movement of dislocations and increase the density of dislocations with the proceeding of tensile process. Therefore, in the later stage of deformation, a large number of dislocation sources in Mg-5Zn alloy can also be initiated even if its grains are fine, which leads to the effective transfer of dislocation slip and the release of stress.

Moreover, Ref. [9] reported that the grain boundary sliding (GBS) can also make a contribution to the reduction of the work hardening rate. However, the effect of the grain size on GBS is considered [39]. Zelin et al. [40] studied the deformation mechanism in a Mg alloy with mixed fine and coarse grains, the results show that GBS is much more pronounced in the fine-grained regions than that with the coarse-grained regions. Therefore, it has been accepted that the tendency of GBS increasing with decreasing grain size [40]. In this work, the average grains size of the as-extruded Mg-5Zn alloy is ~4.11μm, which is much finer than that of pure Mg(~11.89μm), so the contribution of GBS in Mg-5Zn alloy is larger than that in pure Mg. In addition, GBS increases with the increasing strain [39]. The elongation of Mg-5Zn alloy is higher than that of pure Mg in present work. Therefore, according to the above analysis, the contribution of GBS to strain for Mg-5Zn alloy is larger than that of pure Mg. Then, it may be concluded that the recovery trend of Mg-5Zn alloy is larger than that of pure Mg during the tensile process.

Besides, it is generally accepted that the static softening can be driven by the stored energy generated during plastic deformation, which is also related to the work hardening effect [41]. Chen et al. [18] reported that the existence of Al_3Zr dispersoids in Al-Zn-Mg-Cu alloy can play a stronger role in the inhibition of dynamic recovery during deformation, which will provide driving force for static softening. Besides, their research also found that the more Al_3Zr dispersions would be generated in Al-Zn-Mg-Cu alloy with the increasing Zr contents, which could not only pin dislocations and result in the higher strain energy, but also provide much higher driving force for subsequent static softening [18]. The same things were also confirmed in Lianos et al's investigation [42]. Therefore, the driving forces of softening may be affected by the stored energy produced during deformation. In this work, the work hardening rate of pure Mg is larger than that of Mg-5Zn alloy in the early stage of deformation, as shown in Fig. 9(d). Then, the stored energy and driving force of softening for pure Mg are larger than that of Mg-5Zn alloy in the early stage of deformation, which leads to the higher value of $\triangle P_1$ for pure Mg as compared with Mg-5Zn alloy. However, Mg-5Zn alloy possesses a higher work hardening rate than pure Mg in the later stage of deformation (Fig. 9(d)), which indicates that Mg-5Zn alloy may has higher stored energy and larger softening driving force in the later stage of deformation. Therefore, when the tensile displacement remains unchanged at the later stage of deformation, the values of $\triangle P_1$ and $\triangle P_2$ for Mg-5Zn alloy increase obviously.

5. Conclusions

In this paper, the line broadening evolution of pure Mg and Mg-5Zn alloy during

in-situ tension were meansured by neutron diffraction, and the dynamic recovery at different deformation stages during tension were calculated and anylyzed, the effect of the grain size and precipitation on the work hardening and softening behavior was studied. The conclusions can be summaried as follows:

(1) The average DRXed size and DRXed ratio of Mg-5Zn alloy are smaller than that of pure Mg due to the pinning effect of precipitates on grain boundary migration and retarding DRX, resluting in a high mechanical properties are achieved by Mg-5Zn alloy.

(2) The work hardening rate of pure Mg is larger than Mg-5Zn alloy in the early stage of deformation due to the effect of grain size on the work hardeing is stronger than precipitates. However, Mg-5Zn alloy possesses higher work hardening rate in the later deformation stage, which is attributed to the stonger effect of precipitates on work hardening behaivor.

(3) The contribution of GBS in Mg-5Zn alloy is greater than pure Mg during tensile, which makes the softening effect of Mg-5Zn alloy larger than that of pure Mg.

(4) Stored energy generated during tensile deformation can provide the driving force of softening for pure Mg and Mg-5Zn alloy. The higher stored energy of pure Mg in the early stage of deformation leads to higher $\triangle P_1$ value. However, the stored energy of Mg-5Zn alloy increases rapidly with the increase of tensile strain, resulting in the increase of softening effect in the later deformation stage.

Acknowledgment

This work was supported by “National Natural Science Foundation of China” (Grants. 51771128 and 51771129), Projects of International Cooperation in Shanxi (Grant no. 201703D421039), and the Program for the Outstanding Innovative Teams of Higher Learning Institutions of Shanxi.

References

[1] Y.D. Qiao, X. Wang, Z.Y. Liu, E. Wang, Effect of temperature on microstructures, texture and mechanical properties of hot rolled pure Mg sheets, Mater. Sci. Eng. A 568(4) (2013) 202-205.

[2] B.P. Zhang, Y. Wang, L. Geng, C.X. Lu, Effects of calcium on texture and mechanical properties of hot-extruded Mg–Zn–Ca alloys, Mater. Sci. Eng. A 539(2) (2012) 56-60.

[3] T. Tański, L.A. Dobrzański, L. Čížek, Influence of Heat Treatment on Structure and Properties of the Cast Magnesium Alloys, Adv. Mater. Res 15-17(2) (2007) 491-496.

[4] H. Somekawa, T. Mukai, Effect of texture on fracture toughness in extruded AZ31 magnesium alloy, Scr. Mater 53(5) (2005) 541-545.

[5] J. Koike, T. Kobayashi, T. Mukai, H. Watanabe, M. Suzuki, K. Maruyama, K. Higashi, The activity of non-basal slip systems and dynamic recovery at room temperature in fine-grained AZ31B magnesium alloys, Acta Mater 51(7) (2003) 2055-2065.

[6] T.T. Liu, F.S. Pan, X.Y. Zhang, Effect of Sc addition on the work-hardening behavior of ZK60 magnesium alloy, Mater. Des 43 (2013) 572-577.

[7] Y.K. Kim, S.W. Sohn, D.H. Kim, W.T. Kim, D.H. Kim, Role of icosahedral phase in enhancing the strength of Mg–Sn–Zn–Al alloy, J. Alloy Compd 549(2) (2013) 46-50.

[8] B. Rashkova, W. Prantl, R. Görgl, J. Keckes, S. Cohen, M. Bamberger, G. Dehm, Precipitation processes in a Mg–Zn–Sn alloy studied by TEM and SAXS, Mater. Sci. Eng. A 494(1-2) (2008) 158-165.

[9] J.A. del Valle, F. Carreño, O.A. Ruano, Influence of texture and grain size on work hardening and ductility in magnesium-based alloys processed by ECAP and rolling, Acta Mater 54(16) (2006) 4247-4259.

[10] L.L. Guo, Z.C. Chen, L. Gao, Effects of grain size, texture and twinning on mechanical properties and work-hardening behavior of AZ31 magnesium alloys, Mater. Sci. Eng. A 528(29-30) (2011) 8537-8545.

[11] C.Y. Zhao, X.H. Chen, F.S. Pan, J.F. Wang, S.Y. Gao, T. Tu, C.Q. Liu, J.H. Yao, A. Atrens, Strain hardening of as-extruded Mg-*x*Zn (*x* = 1, 2, 3 and 4 wt%) alloys, J. Mater. Sci. Tech 35(1) (2019) 142-150.

[12] X.Z. Lin, D.L. Chen, Strain Hardening and Strain-Rate Sensitivity of an Extruded Magnesium Alloy, J. Mater. Eng. Perform 17(6) (2008) 894-901.

[13] L. Zhang, K.K. Deng, Microstructures and mechanical properties of SiC_p/Mg-xAl-2Ca composites collectively influenced by SiC_p and Al content, Mater. Sci. Eng. A 725 (2018) 510-521.

[14] M. Habibnejad-Korayem, R. Mahmudi, W.J. Poole, Work hardening behavior of Mg-based nano-composites strengthened by Al_2O_3 nano-particles, Mater. Sci. Eng. A

567 (2013) 89-94.

[15] X.S. Li, L.Z. Wu, J. Chen, H.B. Zhang, Static Softening Characteristics and Static Recrystallization Kinetics of Aluminum Alloy A6082 After Hot Deformation, J. Shanghai Jiaotong Univ. (Sci.) 15(3) (2010) 307-312.

[16] F.L. Jiang, H. Zhang, L.X. Li, J.H. Chen, The kinetics of dynamic and static softening during multistage hot deformation of 7150 aluminum alloy, Mater. Sci. Eng. A 552 (2012) 269-275.

[17] F. Jiang, H.S. Zurob, G.R. Purdy, Z. Hui, Static softening following multistage hot deformation of 7150 aluminum alloy: Experiment and modeling, Mater. Sci. Eng. A 648 (2015) 164-177.

[18] K.Y. Chen, J. Tang, F.L. Jiang, J. Teng, D.F. Fu, H. Zhang, The role of various Zr additions in static softening behavior of Al-Zn-Mg-Cu alloys during interval holding of double-stage hot deformation, J. Alloy Compd. 792 (2019) 1112-1121.

[19] C. Chao, J.H. Chen, H.G. Yan, B. Su, S. Min, S.Q. Zhu, Dynamic precipitation, microstructure and mechanical properties of Mg-5Zn-1Mn alloy sheets prepared by high strain-rate rolling, Mater. Des 100 (2016) 58-66.

[20] S. Jing, S. Kaboli, A.S.H. Kabir, I.H. Jung, S. Yue, Effect of dynamic precipitation and twinning on dynamic recrystallization of micro-alloyed Mg–Al–Ca alloys, Mater. Sci. Eng. A 587(1) (2013) 27-35.

[21] S.H. Kim, J.H. Lee, C.S. Lee, J. Yoon, S.H. Park, Dynamic deformation behavior and microstructural evolution during high-speed rolling of Mg alloy having non-basal texture, J. Mater Sci. Tech 35(4) (2019) 473-482.

[22] H. Borkar, R. Gauvin, M. Pekguleryuz, Effect of extrusion temperature on texture evolution and recrystallization in extruded Mg–1% Mn and Mg–1% Mn–1.6%Sr alloys, J. Alloy Compd 555(1) (2013) 219-224.

[23] D.K. Guan, W.M. Rainforth, L. Ma, B. Wynne, J.H. Gao, Twin recrystallization mechanisms and exceptional contribution to texture evolution during annealing in a magnesium alloy, Acta Mater 126 (2017) 132-144.

[24] É. Martin, R.K. Mishra, J.J. Jonas, Effect of twinning on recrystallisation textures in deformed magnesium alloy AZ31, Philos. Mag 91(27) (2011) 3613-3626.

[25] T.S. Zhao, Y.B. Hu, B. He, C. Zhang, T.X. Zheng, F.S. Pan, Effect of manganese on microstructure and properties of Mg-2Gd magnesium alloy, Mater. Sci. Eng. A 765(2019) 138292.

[26] T. Ungár, M. Zehetbauer, Stage IV work hardening in cell forming materials, part II: A new mechanism, Scr. Mater 35(12) (1996) 1467-1473.

[27] L. Zhang, K.K. Deng, K.B. Nie, F.J. Xu, K. Su, W. Liang, Microstructures and mechanical properties of Mg–Al–Ca alloys affected by Ca/Al ratio, Mater. Sci. Eng. A 636 (2015) 279-288.

[28] N. Afrin, D.L. Chen, X. Cao, M. Jahazi, Strain hardening behavior of a friction stir welded magnesium alloy, Scr. Mater 57(11) (2007) 1004-1007.

[29] X.H. Chen, F.S. Pan, J.J. Mao, J.F. Wang, D.F. Zhang, A.T. Tang, P. Jian, Effect of heat treatment on strain hardening of ZK60 Mg alloy, Mater. Des 32(3) (2011) 1526-1530.

[30] F. Bo, Y.C. Xin, F.L. Guo, H.H. Yu, W. Yang, Q. Liu, Compressive mechanical

behavior of Al/Mg composite rods with different types of Al sleeve, Acta Mater 120 (2016) 379-390.

[31] S.M. Chowdhury, D.L. Chen, S.D. Bhole, X. Cao, E. Powidajko, D.C. Weckman, Y. Zhou, Tensile properties and strain-hardening behavior of double-sided arc welded and friction stir welded AZ31B magnesium alloy, Mater. Sci. Eng. A 527(12) (2010) 2951-2961.

[32] G.S. Hu, D.F. Zhang, D.Z. Zhao, L.Y. Jiang, D.L. Yu, F.S. Pan, Work-Hardening Behavior of ZMT614-xY(x=0, 0.1, 0.5, 1.0) Magneisum Alloy, Rare. Met. Mater. Eng 44(2015) 2015-2019.

[33] D.D. Zhang, D.P. Zhang, F.Q. Bu, X.L. Li, B.S. Li, T.L. Yan, K. Guan, Q. Yang, X.J. Liu, J. Meng, Excellent ductility and strong work hardening effect of as-cast Mg-Zn-Zr-Yb alloy at room temperature, J. Alloy Compd 728 (2017) 404-412.

[34] E.L.S. Solomon, A.R. Natarajan, A.M. Roy, V. Sundararaghavan, A. Van der Ven, E.A. Marquis, Stability and strain-driven evolution of β′ precipitate in Mg-Y alloys, Acta Mater 166 (2019) 148-157.

[35] H.D. Fan, Y.X. Zhu, J.A. El-Awady, D. Raabe, Precipitation hardening effects on extension twinning in magnesium alloys, Int. J. Plast 106 (2018) 186-202.

[36] X.Y. Xia, W.H. Sun, A.A. Luo, D.S. Stone, Precipitation evolution and hardening in Mg-Sm-Zn-Zr alloys, Acta Mater 111 (2016) 335-347.

[37] D.S. Wang, M. Amsler, V.I. Hegde, J.E. Saal, A. Issa, B.-C. Zhou, X.Q. Zeng, C. Wolverton, Crystal structure, energetics, and phase stability of strengthening precipitates in Mg alloys: A first-principles study, Acta Mater 158 (2018) 65-78.

[38] X.H. Chen, L. Lu, K. Lu, Grain size dependence of tensile properties in ultrafine-grained Cu with nanoscale twins, Scr. Mater 64(4) (2011) 311-314.

[39] J. Koike, R. Ohyama, T. Kobayashi, M. Suzuki, K. Maruyama, Grain-Boundary Sliding in AZ31 Magnesium Alloys at Room Temperature to 523K, Mater. Trans 44(4) (2003) 445-451.

[40] M.G. Zelin, H.S. Yang, R.Z. Valiev, A.K. Mukherjee, Interaction of high-temperature deformation mechanisms, Metall. Trans. A 23(11) (1992) 3135-3140.

[41] F.J. Humphreys, M. Hatherly, Recrystallization and related annealing phenomena, ELSEVIER Ltd, Kidlington, 1995, pp. 219-224.

[42] L. Llanos, B. Pereda, B. Lopez, J.M. Rodriguez-Ibabe, Hot deformation and static softening behavior of vanadium microalloyed high manganese austenitic steels, Mater. Sci. Eng. A 651 (2016) 358-369.